

A High-throughput Assessing of Adsorption Capacity and Li-ion Diffusion Dynamics in Mo Based Ordered Double-Transition-Metal MXenes as Anode Materials for Fast Charging LIBs

Hangyu Wang^a, Ziang Jing^a, Haoliang Liu^a, Xianghui Feng^a, Guodong Meng^a,

Kai Wu^a, Yonghong Cheng^a, Bing Xiao^{*a}

a. School of Electrical Engineering, State Key Laboratory of Electrical Insulation and Power Equipment, Xi'an Jiaotong University, Xi'an 710049, China

Corresponding Author: bingxiao84@xjtu.edu.cn

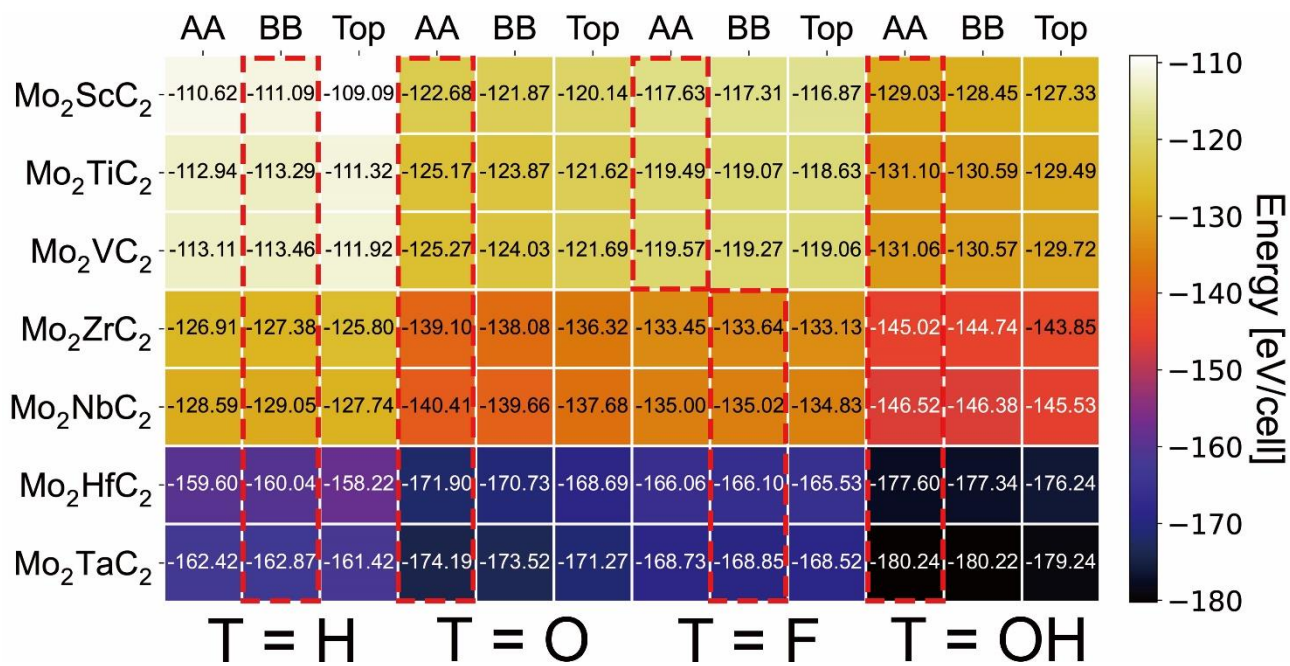


Figure S1. The total energies of Mo-based MXenes with surface functional groups T (H, O, F, and OH) at different adsorption sites. The most stable adsorption structures and associated total cell energies are highlighted in rectangular box by the red-dashed lines.

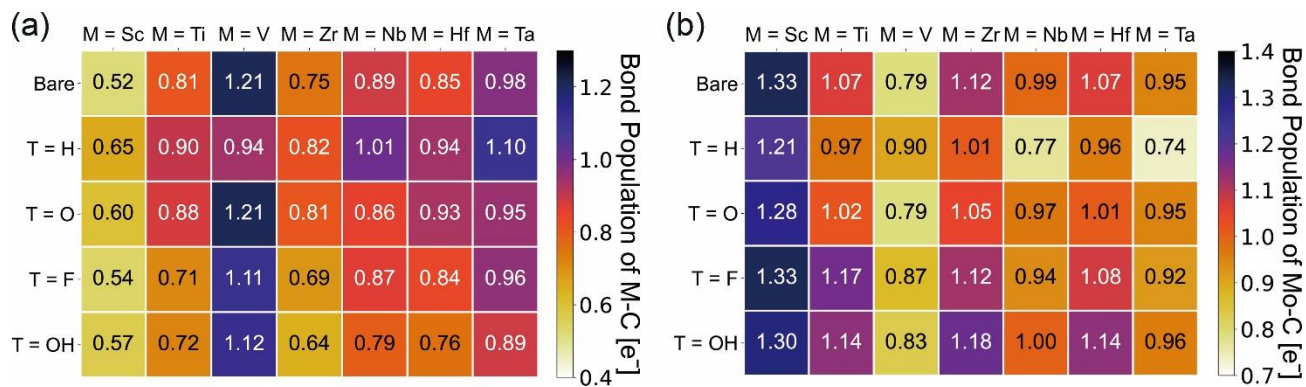


Figure S2. The bond population of (a) M-C and (b) Mo-C in Mo_2MC_2 and $\text{Mo}_2\text{MC}_2\text{T}_2$ ($M = \text{Sc, Ti, V, Zr, Nb, Hf, Ta}$, $T = \text{H, O, F, OH}$).

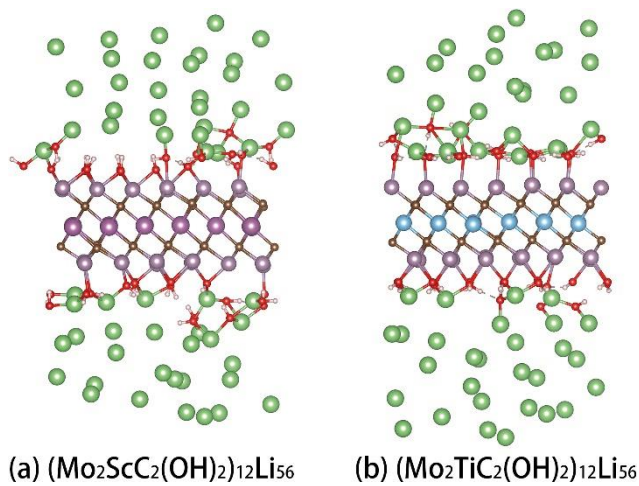


Figure S3. The snapshots of -OH functionalized MXenes placed in between two bulk Li metals in FPMD simulations at 200 K: (a) Mo_2ScC_2 and (b) Mo_2TiC_2 .

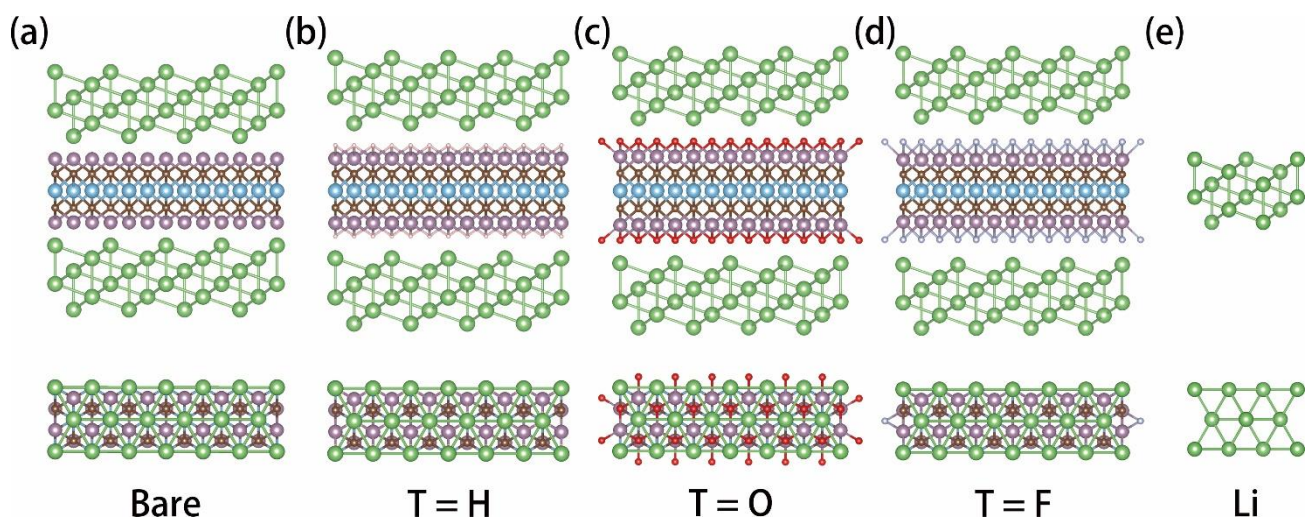


Figure S4. The top and side view of initial sandwich structures of (a) Mo_2MC_2 , (b) $\text{Mo}_2\text{MC}_2\text{H}_2$, (c) $\text{Mo}_2\text{MC}_2\text{O}_2$, (d) $\text{Mo}_2\text{MC}_2\text{F}_2$ and the crystallographic plane (111) of bulk Li metal (BCC).

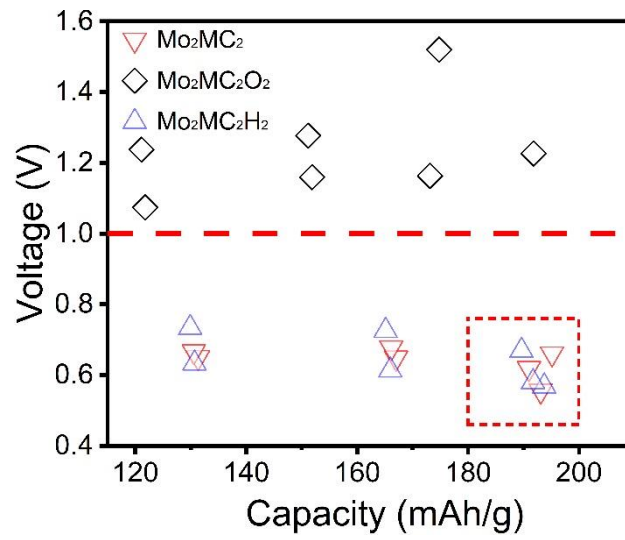


Figure S5. Average open circuit voltage and theoretical capacity of Li saturated adsorption structures of Mo₂MC₂ and Mo₂MC₂T₂ (M stands for transition metal, and T = H, and O). The red box area indicates an optimal active voltage window and with storage capacity greater than 180 mAh/g.

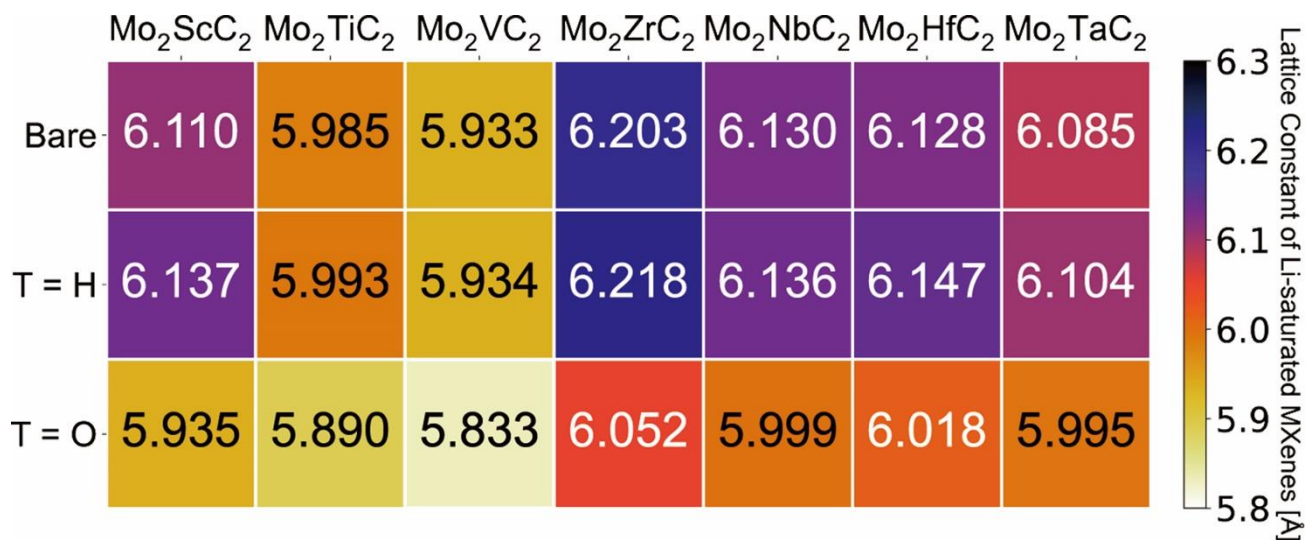
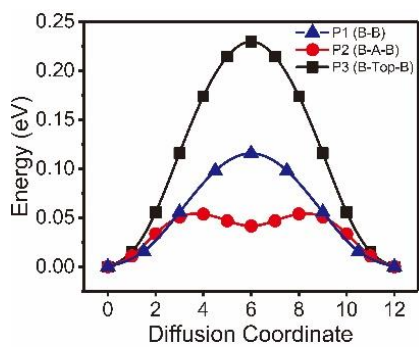
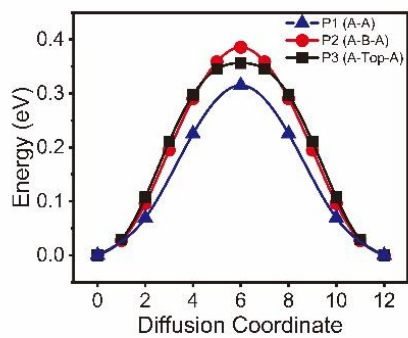


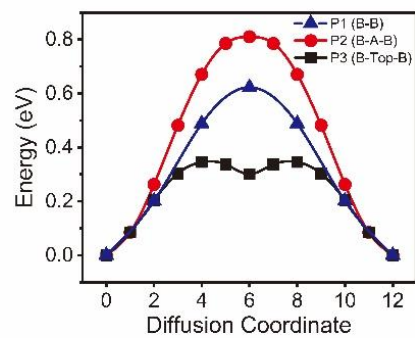
Figure S6. Planar lattice constants of 2×2×1 supercell model of Mo₂MC₂, Mo₂MC₂H₂ and Mo₂MC₂O₂ (M = Sc, Ti, V, Zr, Nb, Hf, Ta) with full Li adsorbed.



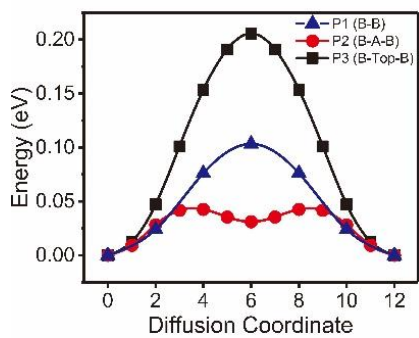
(a) Mo_2ScC_2



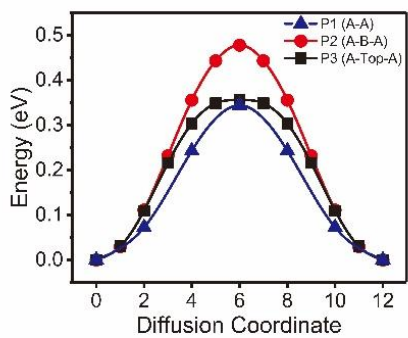
(b) $\text{Mo}_2\text{ScC}_2\text{H}_2$



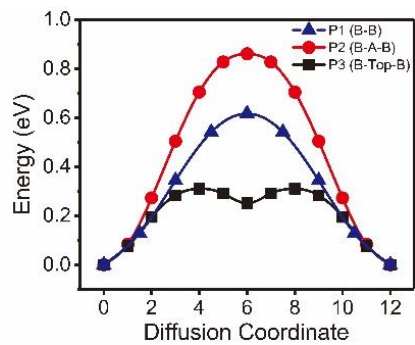
(c) $\text{Mo}_2\text{ScC}_2\text{O}_2$



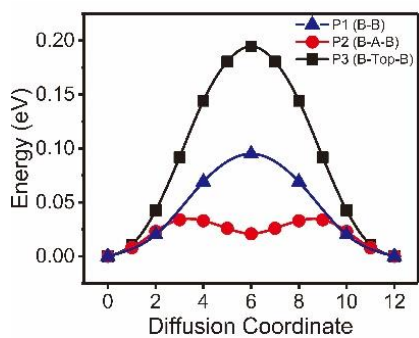
(d) Mo_2TiC_2



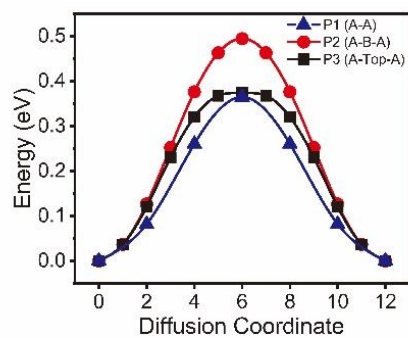
(e) $\text{Mo}_2\text{TiC}_2\text{H}_2$



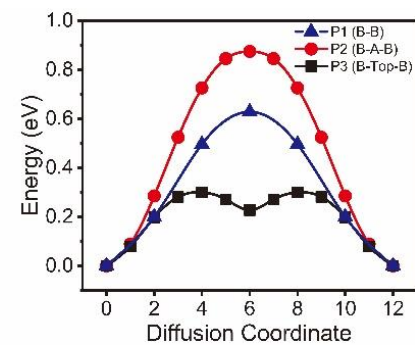
(f) $\text{Mo}_2\text{TiC}_2\text{O}_2$



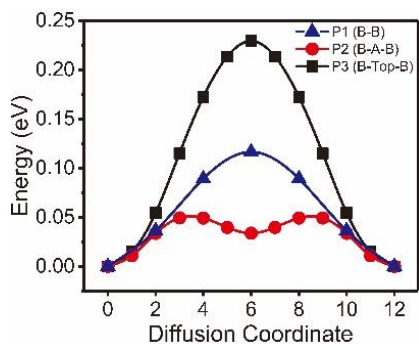
(g) Mo_2VC_2



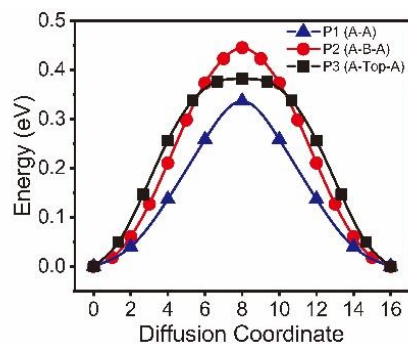
(h) $\text{Mo}_2\text{VC}_2\text{H}_2$



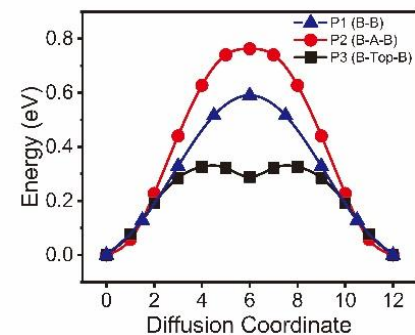
(i) $\text{Mo}_2\text{VC}_2\text{O}_2$



(j) Mo_2ZrC_2



(k) $\text{Mo}_2\text{ZrC}_2\text{H}_2$



(l) $\text{Mo}_2\text{ZrC}_2\text{O}_2$

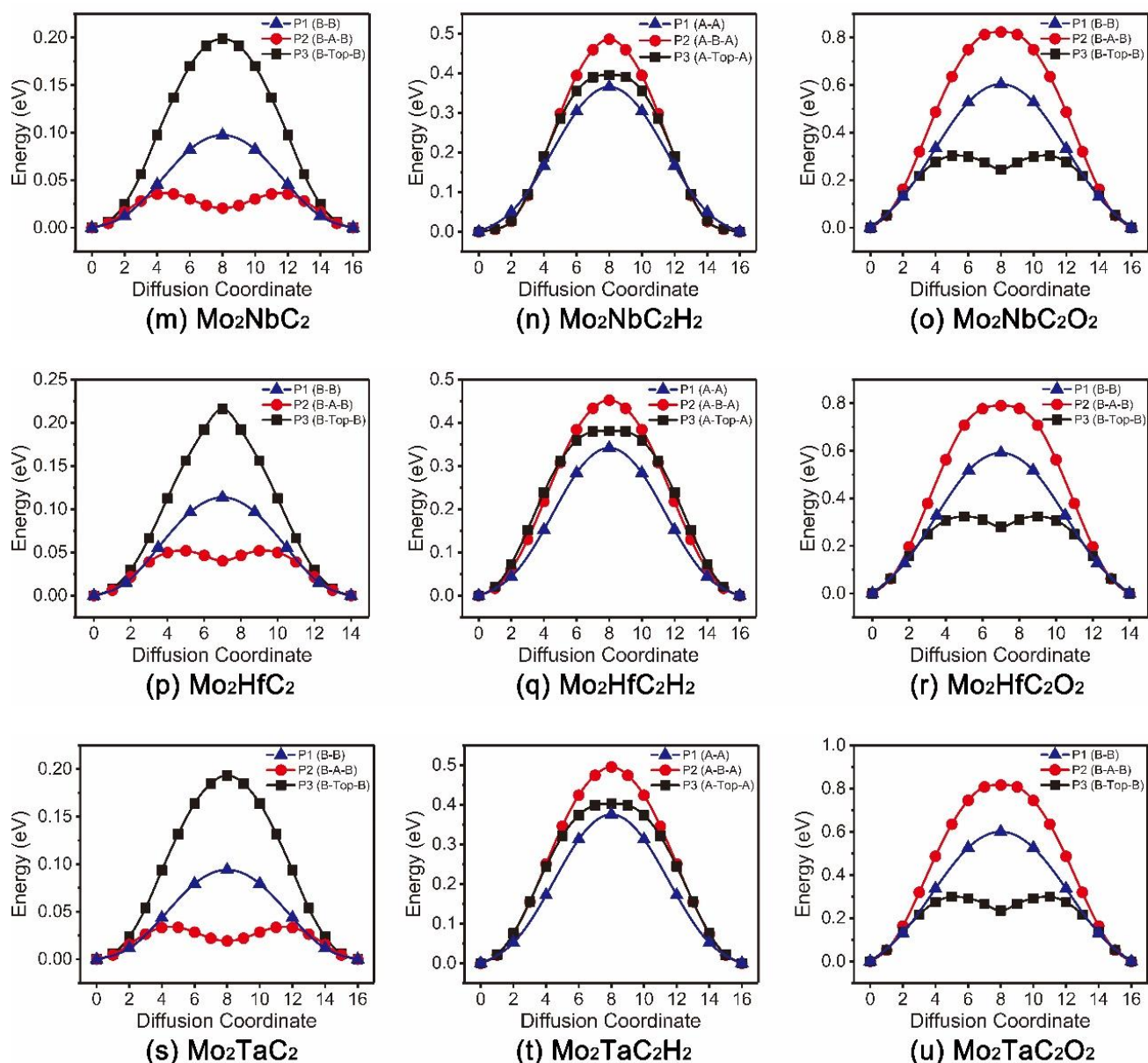


Figure S7. Diffusion energy profiles of Li-ion for Mo_2MC_2 and $\text{Mo}_2\text{MC}_2\text{T}_2$ ($M = \text{Sc}, \text{Ti}, \text{V}, \text{Zr}, \text{Nb}, \text{Hf}, \text{Ta}$, and $T = \text{H}, \text{O}$) MXenes, calculated using a $2 \times 2 \times 1$ supercell model.

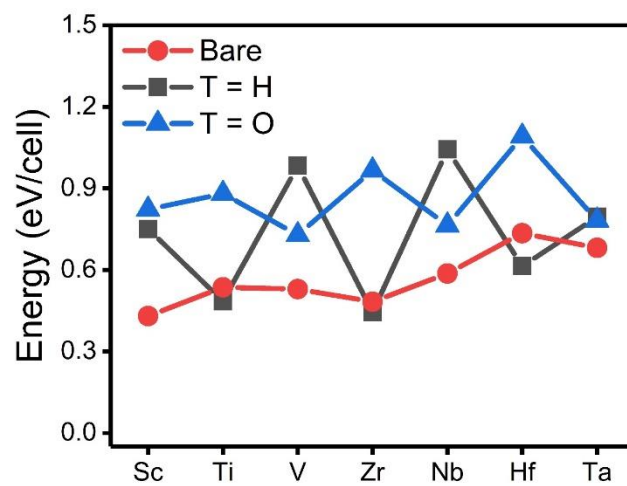


Figure S8. Formation energy of a Li vacancy in saturated adsorption structures $(\text{Mo}_2\text{MC}_2)_4\text{Li}_8$ and $(\text{Mo}_2\text{MC}_2\text{T}_2)_4\text{Li}_8$ ($\text{T} = \text{H}, \text{O}$).

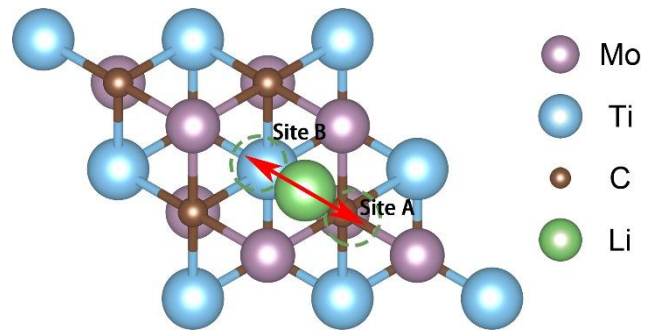


Figure S9. The phonon eigenvector of the soft mode at Γ -point for lithium atom at the saddle point. The direction of the vibration is the same as that of the diffusion.

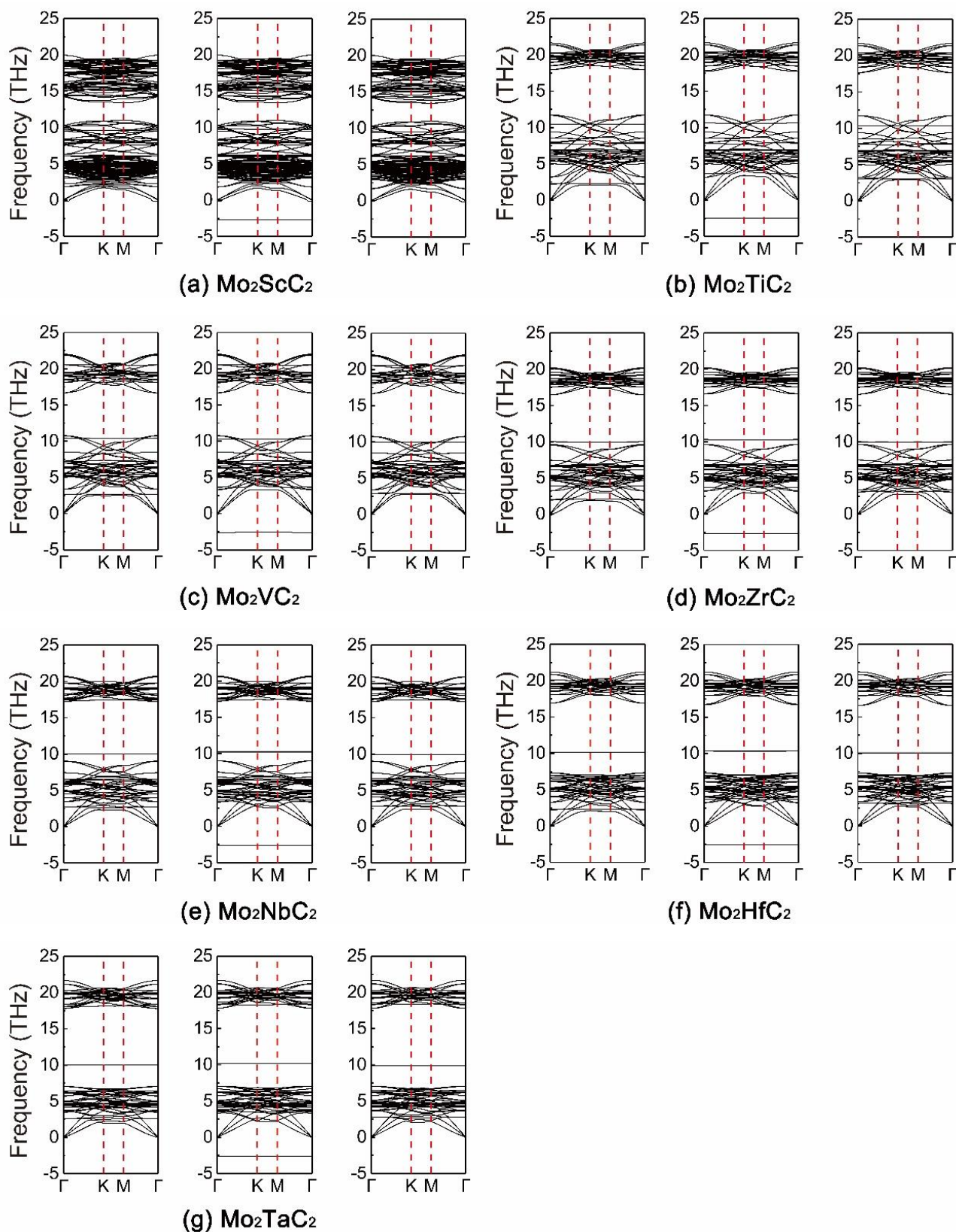


Figure S10. Calculated phonon band vibrational spectra of $\text{Li}-(\text{Mo}_2\text{MC}_2)_4$ ($M = \text{Sc}, \text{Ti}, \text{V}, \text{Zr}, \text{Nb}, \text{Hf}, \text{Ta}$) at the global energy minimum, the saddle-point, and metastable state on the diffusion pathways. Soft modes are displayed as the horizontal lines below 0 THz for all structure at saddle-point.

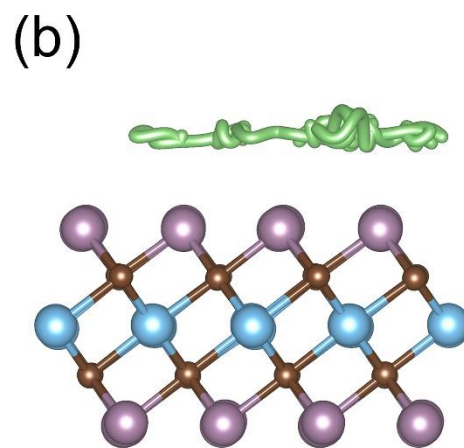
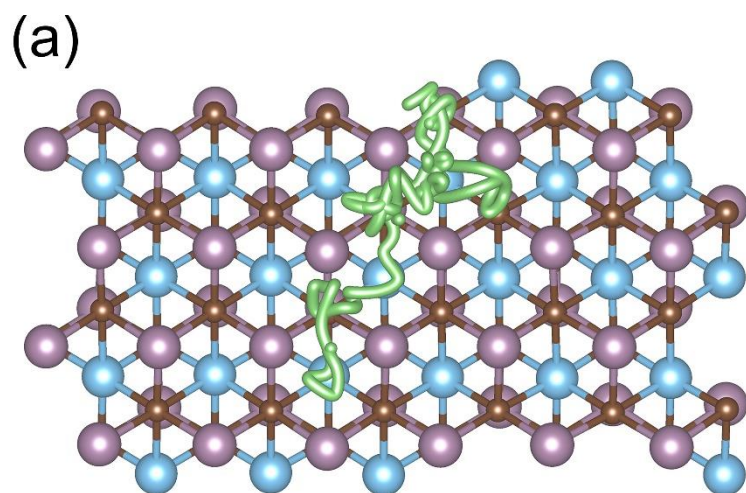


Figure S11. (a) Top view and (b) side view of the migration pathway of Li atom from FPMD simulation for Mo₂TiC₂ monolayer at 400K.

Table S1. The adsorption energies E_{ab} of Li atoms on Mo_2ScC_2 and $\text{Mo}_2\text{ScC}_2\text{T}_2$ with spin-polarized and non-spin-polarized calculations.

	Adsorption energy (eV/cell)	
	Spin-polarized	Non-spin-polarized
Mo_2ScC_2	-0.74	-0.74
$\text{Mo}_2\text{ScC}_2\text{H}_2$	-0.438	-0.440
$\text{Mo}_2\text{ScC}_2\text{O}_2$	-3.05	-3.05
$\text{Mo}_2\text{ScC}_2\text{F}_2$	-0.158	-0.159
$\text{Mo}_2\text{ScC}_2(\text{OH})_2$	0.66	0.66

Table S2. The bond lengths of Mo-C and C-M bonds for embedded MXene layers in between two overlayers after FPMD simulations ((Mo₂MC₂F₂)₁₂Li₄₈).

	$d_{\text{Mo-C}} (\text{\AA})$	$d_{\text{C-M}} (\text{\AA})$	$d_{\text{Mo-F}} (\text{\AA})$
Mo ₂ ScC ₂ F ₂	2.15	2.28	3.63
Mo ₂ TiC ₂ F ₂	2.13	2.16	3.72
Mo ₂ VC ₂ F ₂	2.09	2.07	3.86
Mo ₂ ZrC ₂ F ₂	2.20	2.38	-
Mo ₂ NbC ₂ F ₂	2.09	2.25	-
Mo ₂ HfC ₂ F ₂	2.11	2.25	-
Mo ₂ TaC ₂ F ₂	2.10	2.17	3.37

Table S3. The soft mode frequencies, diffusion barrier heights and corresponding diffusion coefficient obtained from TST+DFPT method, based on CI-NEB migration pathways for all intrinsic MXenes.

	Virtual frequency (THz)	Barrier height (eV)	Diffusion coefficient (m ² /s)
Mo ₂ ScC ₂	-2.678	0.055	2.54×10 ⁻⁸
Mo ₂ TiC ₂	-2.466	0.043	3.14×10 ⁻⁸
Mo ₂ VC ₂	-2.582	0.034	4.25×10 ⁻⁸
Mo ₂ ZrC ₂	-2.639	0.049	2.46×10 ⁻⁸
Mo ₂ NbC ₂	-2.646	0.036	4.36×10 ⁻⁸
Mo ₂ HfC ₂	-2.508	0.052	2.60×10 ⁻⁸
Mo ₂ TaC ₂	-2.598	0.033	4.42×10 ⁻⁸

Table S4. Comparison of diffusion coefficients of Li atoms calculated for Mo_2MC_2 (M = Sc, Ti, V) at 400K using TST+DFPT and FPMD simulations.

	Diffusion coefficient (m^2/s)		
	Mo_2ScC_2	Mo_2TiC_2	Mo_2VC_2
TST analysis	4.21×10^{-8}	4.35×10^{-8}	5.70×10^{-8}
FPMD	6.36×10^{-9}	2.70×10^{-9}	9.77×10^{-9}